African Journal of Applied Research
Vol. 12, No. 3 (2026), pp. 315-340
http://www.ajaronline.com
https://doi.org/10.26437/ajar.v12
Received May 3, 2025
Peer reviewed: December 12, 2025
Revised: February 19, 2026
Published: April 2026

AERODYNAMIC PERFORMANCE OPTIMISATION OF A SAVONIUS VAWT FOR TRAFFIC WIND ENERGY HARVESTING

Fawzi Khaleel, H.[1], Al-Kaby, R. N.[2], and Rashid, H. K.[3]
[1,2] *Department of Mechanical Engineering, College of Engineering, University of Babylon, Iraq.*
[3] *Department of Ceramic Engineering, Faculty of Materials Engineering, University of Babylon, Babylon, Iraq.*
[1] *eng883.haithem.fuzy@student.uobabylon.edu.iq*

ABSTRACT

Purpose: This study evaluates the aerodynamic performance of Savonius rotors designed to harvest vehicular kinetic energy at three arterial entrances in Hillah, Iraq.
Design/Methodology/Approach: 36 rotor designs (varying blades: 2, 3, 4; sizes: 4, 6, 8 inches) were tested under simulated urban wind profiles. Empirical results were validated using transient 2D CFD simulations (SST k-w model) within a 5-7% error margin.
Research Limitation: The study is limited to the specific environmental and traffic conditions of Hillah's entrances and relies on 2D CFD simulations.
Findings: A 3-blade, 6-inch design optimally balances torque and drag, achieving a maximum power coefficient (Cp) of 0.545. While 4-inch rotors are aerodynamically efficient, they yield low absolute power; conversely, 8-inch rotors produce high power but suffer from efficiency losses due to vortex shedding. Site-specific optimisations dictate: a 2-blade/4-inch rotor for high velocity (Entrance 1), a 3-blade/6-inch for moderate velocity (Entrance 2), and a 4-blade/6-inch for low velocity (Entrance 3).
Practical Implication: Municipalities can deploy these site-optimised rotors to harness vehicle wakes and sustainably power decentralised infrastructure such as streetlights and traffic sensors.
Social Implication: Generating clean electricity from traffic wakes reduces reliance on traditional power grids, promoting sustainable urban development and localised energy resilience.
Originality / Value: The study provides a novel, scalable approach for topological tuning in harvesting vehicular kinetic energy to power decentralised urban infrastructure.

Keywords: *Aerodynamic. electricity. savonius rotors. traffic. wind turbine*

INTRODUCTION

Climate change and the rapid depletion of fossil resources are forcing a major energy paradigm shift. Solar, geothermal, biomass, and wind energy technologies are essential to decarbonise the world economy and meet exponential energy needs (Ismail et al., 2025). However, adding unstable renewable sources to ageing power infrastructures causes technical and economic issues, such as energy loss during transmission and grid instability. Despite these infrastructure issues, wind energy has become a dominant and competitive energy industry that reduces CO_2 emissions and is as cost-effective as utility-scale solar power (Mohammadi et al., 2018).

ISSN: 2408-7920

African Journal of Applied Research
Vol. 12, No. 3 (2026), pp. 315-340
http://www.ajaronline.com
https://doi.org/10.26437/ajar.v12
Received May 3, 2025
Peer reviewed: December 12, 2025
Revised: February 19, 2026
Published: April 2026

In the main case, the global annual renewable capacity will increase from 666 GW in 2024 to almost 935 GW in 2030. Solar PV and wind are forecasted to account for 95% of all renewable capacity additions through 2030 because their generation costs are lower than for both fossil and non-fossil alternatives in most countries (Blecich et al., 2025). Ambitious macro-level ambitions require energy generation options beyond big, concentrated wind farms. We should reduce our reliance on the grid by using decentralised microgeneration in cities and suburbs.

The anthropogenic wind wake from heavy highway traffic is abundant but underutilised for localised energy generation. Harvesting turbulent, ground-level aerodynamic energy recovers kinetic energy and provides a stable, off-grid power supply for critical roadside infrastructure, such as illumination and surveillance. Harvesting vehicle-induced wakes requires aerodynamic equipment designed for severe fluid dynamics. Figure 1 shows that conventional wind energy converters are basically Horizontal Axis Wind Turbines (HAWTs) and Vertical Axis Wind Turbines (VAWTs).

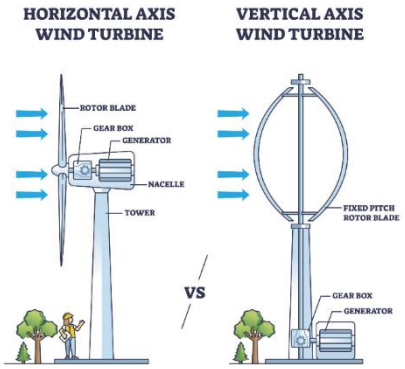

Figure 1: Basic wind energy conversion system classification, comparing HAWTs with VAWTs (El-Ghazali, 2016).

HAWTs are efficient in constant, laminar flow settings, but their high cut-in speed, severe sensitivity to fast direction changes, and complex yaw mechanisms make them unsuitable for highway applications. VAWTs, which can catch wind from any direction, are perfect for harnessing vehicle-generated chaotic, swirling winds (Chen, Chen, & Zhang, 2018).

The aerodynamic configuration of VAWTs is lift-driven (Darrieus) or drag-driven (Savonius). The Savonius rotor has a robust vertical axis geometry with asymmetrically positioned semi-circular buckets (Naseem et al., 2020; Chen et al., 2018). The difference in torque between the advancing blade, which gets flow on its concave surface, and the returning blade, which faces aerodynamic resistance on its convex surface, causes rotation (Montelpare et al., 2018).

The Savonius turbine is ideal for cities because it starts readily in light winds, operates independently of wind direction, requires little maintenance, produces nearly no noise, and blends well with roadside vertical structures. Due to aerodynamic inefficiencies, the Savonius turbine is rarely commercially viable (Alaidany, 2024). The returning blade's significant negative pressure drag severely reduces peak power coefficient (Cp), the main downside.

ISSN: 2408-7920

African Journal of Applied Research
Vol. 12, No. 3 (2026), pp. 315-340
http://www.ajaronline.com
https://doi.org/10.26437/ajar.v12
Received May 3, 2025
Peer reviewed: December 12, 2025
Revised: February 19, 2026
Published: April 2026

Extreme cyclic torque fluctuations in the rotor might cause negative torque output at certain azimuth angles, causing destructive mechanical vibrations and threatening long-term operating stability (Govind, 2017; Akwa et al., 2012). Solving these basic aerodynamic flaws through geometric optimisation is crucial to maximising vehicle wind energy collection.

Rotor Geometry and Parametric Basics

To overcome the aerodynamic limitations reported in the literature, a continuing investigation has focused on optimising the rotor's basic geometry. The aerodynamic efficiency of a Savonius turbine is determined to a very large extent by key design parameters, which include the diameter of the rotor, blade height and overlap ratio as schematically illustrated in Figure 2.

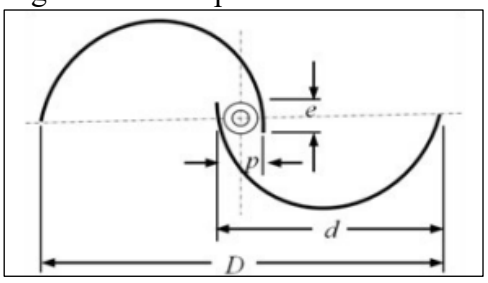

Figure 2: Core geometric design parameters governing the aerodynamic performance of the Savonius vertical-axis rotor (Roy & Saha, 2013).

Furthermore, the number of blades, which determines rotor solidity, has a significant influence on the equilibrium between static starting torque/dynamic performance. Structural variations on two-blade, three-blade and four-blade configurations are given in Figure 3.

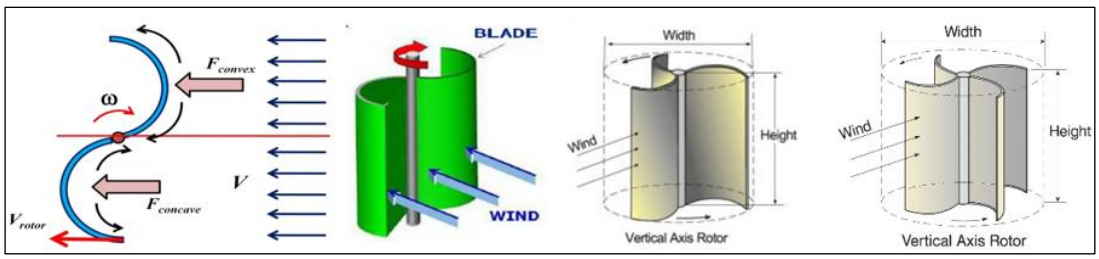

Figure 3: Schematic representation of different Savonius rotor solidities, illustrating the 2-blade, 3-blade, and 4-blade configurations (Gumilar et al., 2019; Ali, 2013).

LITERATURE REVIEW

Blade Profile and Morphological Optimisation

The basic cross-section has been studied to modify Savonius blades to achieve a higher lift-to-drag ratio. (Im & Kim, 2022) studied semicircular, Bach-type, and elliptical shapes and discovered that the semicircular shape provided the optimum stable power production with a maximum efficiency of 18 per cent. Zemamou et al. (2019) demonstrated that a straight back edge enhances aerodynamics with a power coefficient (Cp) of 0.335, being 23% higher than the traditional designs (Faleh et al., 2025).

ISSN: 2408-7920

African Journal of Applied Research
Vol. 12, No. 3 (2026), pp. 315-340
http://www.ajaronline.com
https://doi.org/10.26437/ajar.v12
Received May 3, 2025
Peer reviewed: December 12, 2025
Revised: February 19, 2026
Published: April 2026

Gumilar et al. (2019) have shown that an L-type turbine is extremely energy-capturing and produces 526.39 W at a wind speed of 20 m/s. (Rizaldi & Brahmana, 2024) experimentally verified the use of U-shaped blades and confirmed that this design would work between 3 and 15 m/s wind speeds. (Akhlaghi & Ghafoorian, 2023) discovered that a 180 degrees arc creates optimal torque (Ct=0.501) and power (Cp=0.0261). Kothe et al. (2020) found that a high sweep angle and a low sweep angle of 20 degrees are more effective at improving the lift-to-drag ratio. Recently, Kurniati et al. (2023) have applied CFD to elliptical blades and obtained a Cp of 0.59 at an axis angle of 50 at 9 m/s. Velásquez et al. (2025) used 3-D printing and discovered that the 30-degree blade bending angle is best to increase the aerodynamic efficiency, with the aspect ratio of 2.0, giving Cp=.2326.

Internal Geometric Features: Ratio of Overlaps, Aspect Ratio and the number of blades
Exact rotor dimension requirements are still required to achieve aerodynamic stability. As emphasised by Tania et al. (2018), the overlap ratio (OR) depends on wind speed, with OR = 0.15 at low speeds (less than 4 m/s) and OR = 0.30 at higher, turbulent speeds. Ebrahimpour et al. (2019) presented a multidimensional OR analysis that achieved a 16 per cent improvement. in torque with a horizontal OR of +0.15 and vertical OR of -0.1. Karimi et al. (2023) have highlighted that OR can be optimised depending on the blade type (SR3345 and SR5050) and cautioned that the central rotor shaft may reduce the power factor by interfering with the central airflow. Optimised the number of blades at a tip speed ratio (TSR) of 1.0 using CFD (Dhoble & Mahalle, 2016). Shah and Alsibiani (2020) confirmed the economic viability of a 2-blade rotor with OR=0.1, fabricated from low-cost PVC materials.

Advanced Blade Engineering: Helical Designs, Surface Modifications, and Add-ons
Researchers incorporated modern structural properties to reduce the adverse pull-on returning blades. Rahman, (2018) researched the helical shapes and discovered that 2-bladed and 3-bladed helical designs have better self-starting performance (e.g. 1.4 -1 starting speed in the 3-blade model), and the 2-blade helical shape had the highest Cpk. This was affirmed by Prabowo et al. (2023), who adopted a helical design with a twist angle of 180 degrees to achieve the best cutting speed. Surface texturing also worked remarkably well. Meri Al Absi et al. (2021), found that adding a corrugated inner surface increased Cp by 18. Sumiati et al. (2024), found that a zig-zag pattern on the concave surface increased Cp by 29. Both concepts that were later confirmed by Meri Al Absi et al. (2021), who used a zig -zag surface on the concave surface with OR = 0.2 to obtain Cp = 0.292. Add-ons that can be dynamically adjusted were also studied by Utomo et al. (2018), gained an 11 -percent improvement in Cp by attaching fins to the flow, and (Norouztabar et al., 2022), by 17 percent in torque by incorporating secondary blades and slots. (Farozan & Indartono, 2024), installed check valves in locations close to the tips of the blades to relieve negative returning torque with a performance improvement of 8.7 %.

Flow Augmentation and External Aerodynamic Accessories.
The augmentation strategy of regulating the incoming flow using external accessories is well established. Montelpare et al. (2018) showed that periodic oscillations can be reduced and Cp

ISSN: 2408-7920

African Journal of Applied Research
Vol. 12, No. 3 (2026), pp. 315-340
http://www.ajaronline.com
https://doi.org/10.26437/ajar.v12
Received May 3, 2025
Peer reviewed: December 12, 2025
Revised: February 19, 2026
Published: April 2026

can be increased to approximately 0.30 by fitting self-aligning pneumatic accessories, that is, conveyors and deflectors. Antar & Elkhoury (2019) applied a 3-D CFD to optimise advanced casing and found an increase of 42.5 per cent in the casing at TSR=0.59, and noted that casing dimensions need to change dynamically with different TSRs and not to stay constant. Also, Al-Gburi et al. (2022), minimised blockage effects using flow guided channels (FGC) and corrugated tip zones (WTE) with Cp improvement of 19.5 and 16.8, respectively.

Extensive Reviews and Multi-Parametric research.

Recent in-depth research has combined several parameters at the same time. The effect of aspect ratio, OR, and multistage configurations was synthesised by, and geometric changes could increase efficiency by up to 25. Farajyar et al., (2023) optimised multiple variables and came up with the conclusion that an optimal design with zero OR, 170-degree bow angle and shape factor 0.5 is good. The authors used Design of Experiments (DOE) and CFD in the context of co-optimisation of blade shape, OR and the number of blades to reach 22.8 percent performance improvement (Al-Gburi et al. (2023) . Lastly, intensive assessments conducted by Fanel Dorel et al. (2021) summarised the fundamental effect of integrating internal alterations with exterior accessories (e.g. endplates and curtains), as these combined alterations may enhance the power coefficient by more than 38.5.

Research Gap and Present Contribution

Even though there have been numerous studies on Savonius designs, there is still an important lack of research on how these specific setups perform in low-speed, highly turbulent, and changing wind generated by vehicles. Therefore, this study tests how well a small Savonius VAWT captures wind generated by cars. Using actual wind speed data (4-8 m/s) collected from main roads in Hillah City, Iraq, this research examines the effects of varying rotor size and blade number. The main goal is to find the best turbine design that can extract the most energy from this unusual, constant wind source.

The rest of this paper is organised as follows: Section 2 specifies the methodology of the experiment, including the steps for data acquisition in the field, the geometric testing matrix, and the implementation of the novel near-zero-friction spindle. Section 3 describes the numerical framework, including the 2D CFD domain, the governing equations, and the validation strategy. Section 4 provides a comprehensive discussion of the results: the parameters of the blades (number and diameter) and aerodynamic saturation are analysed, and the physical justification for the unattenuated efficiency measures is offered. Finally, Section 5 summarises the main conclusions that are drawn from this investigation.

METHODOLOGY

Vertical wind turbine model

All experiments for all VAWT cases in this study were carried out in the post-graduate laboratories of the College of Engineering/University of Babylon, at ambient conditions of (37 °C) and pressure of 100.2 kPa. The experimental work was conducted to design a VAWT of

African Journal of Applied Research
Vol. 12, No. 3 (2026), pp. 315-340
http://www.ajaronline.com
https://doi.org/10.26437/ajar.v12
Received May 3, 2025
Peer reviewed: December 12, 2025
Revised: February 19, 2026
Published: April 2026

two blades, as shown in Plate 1. The blades are made of polyvinyl chloride (PVC) of 4 mm thickness by three different diameter blades (8,6,4) inches, and all the blades are 37 cm in height.

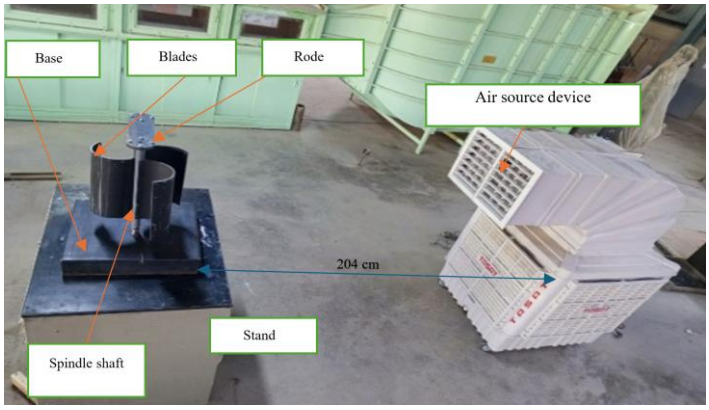

Plate 1: Current model of Savinous VAWT (Experimental setup).

Experimentally measuring vehicle-induced air flow velocities at three Hillah city entrances. The velocity ranges were (6–8) m/s at Entry 1, (5–7) m/s at Entry 2, and (4-5) m/s at Entry 3. An experimental investigation using an air-producing device to simulate air velocity ranges found the optimal design. We built several small vertical wind turbines with different blade counts and rotating shaft diameters to find the best configuration for each location to maximise traffic-generated wind energy transfer. Turbine rods are plastic tubes on spindles used for high-speed spinning machines. Plate 2 shows why it is a basic element in the Savonius rotor: it is easy to install, move, bear the weight, and is free of friction and vibration during rotation, making it self-moving in low winds. Details of turbine parts, blades, spindle shaft, and ball-bearing end.

(a)

(b)

Plate 2: (a) Savinuos wind turbine parts (b) shows the spindle shaft with a ball bearing.

ISSN: 2408-7920

African Journal of Applied Research
Vol. 12, No. 3 (2026), pp. 315-340
http://www.ajaronline.com
https://doi.org/10.26437/ajar.v12
Received May 3, 2025
Peer reviewed: December 12, 2025
Revised: February 19, 2026
Published: April 2026

Setting screws attached the blades to a spindle for the small vertical wind turbine. The spindle's blades are different sizes and attached to an iron rod. The top of the spindle screws into the ball-bearing base. A bushing on the spindle top secures this bearing for smooth rotation. A 58 cm street lamp pole with two rings secures the ball bearing and welds this upper assembly. The experimental tests simulated car wind using a large air-source device (Plate 2). It was 204 cm from the turbine and controlled remotely to match the air speed to the road entry velocity. Plate 3 (a) shows 2 savinuos VAWT blades for 4-inch blade diameter, 3(b) shows 3 blades, and **Error! Reference source not found.** (c) shows 4 blades. Plate 3 (d) shows all blades screwed behind the shaft and three and four fixed to its outer surface on both sides of the shaft.

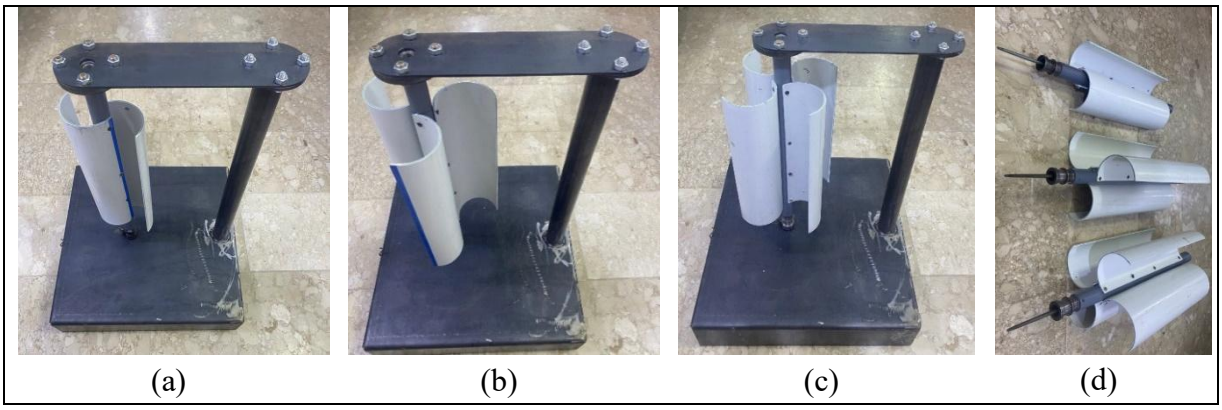

Plate 3: Savinuos 4-inch diameter. (a) 2 blades (b) 3 blades (c) 4 blades. (d) shows the spindle shaft with different numbers of blades.

Typically, the diameter of the blade is also changed to (8) and (6) inches, and all experiments are repeated with those diameters for two, three, and four blades (Plate 4).

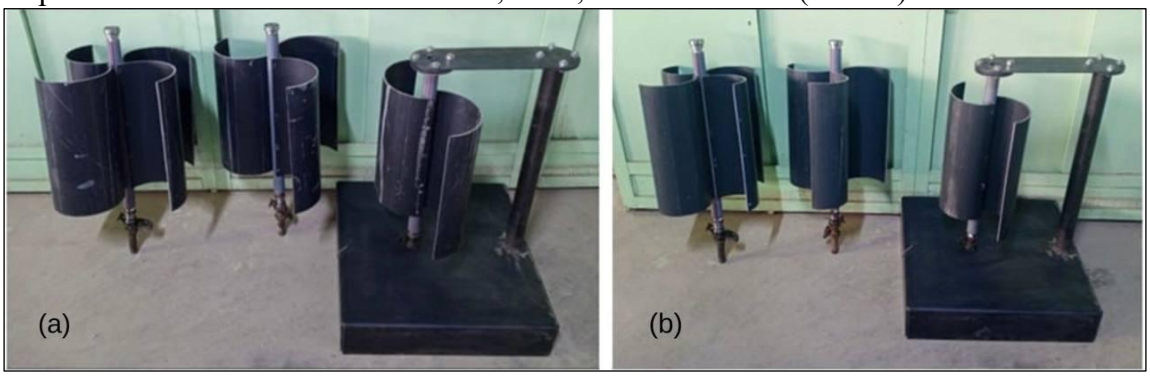

Plate 4: Savinous 2, 3, and 4 blades, (a) 8-inch diameter (b) 6-inch diameter.

An anemometer connected to a remote control controlled the air source device's air flow velocity (Plate 5-a). Table 1 shows the study turbine's design properties. Three Hilla city inlets measured air wind velocities.

ISSN: 2408-7920

African Journal of Applied Research
Vol. 12, No. 3 (2026), pp. 315-340
http://www.ajaronline.com
https://doi.org/10.26437/ajar.v12
Received May 3, 2025
Peer reviewed: December 12, 2025
Revised: February 19, 2026
Published: April 2026

Table 1: The VAWT model's geometric properties.

Properties	Value	Units
Blades number	2,3,4	-
Height of the blade	37	cm
Diameter of the blade	8"(20), 6"(15) ,4" (10)	inch (cm)
Radius of rotor (3,4)- blades	R=d + (e/2)	cm
Radius of rotor 2-blades	R=d - (e/2) – t	cm
Wind speed	4, 5,6, 7, and 8	m/s
Diameter of shaft	3.3	cm
Radius of the bottom Spindel	11.5	mm
Thickness of the blade	4	mm

Each entrance received 60 air velocity readings from the left side of the road for 60 minutes (**Error! Reference source not found.** 5-a). The experiment used an RPM device to measure rotational speed (Plate 5-b), a spring scale to calculate torque (Plate 5-c), and a Vernier calliper for precise dimensional measurements. Plate 5-e shows the air source drive accurately simulating the traffic wind.

(a) (b) (c) (d) (e)

Plate 5: (a) Anemometry device, (b) Digital Tachometer, (c) Force meter, (d) Vernier Calliper, and (e) Air source device with remount control.

Performance Parameters

Wind energy is simply the kinetic energy of massive air masses travelling across Earth. Kinetic energy becomes mechanical or electric. Rotor-wind interaction efficiency affects wind conversion efficiency to mass energy. This work begins with wind energy conversion theory. Air with mass (m) moves at velocity (V), so its kinetic energy (E) is:

$$\mathbf{E = \frac{1}{2}mV^2 = \frac{1}{2}\rho_a vV^2} \quad \textbf{(1)}$$

In a wind stream, the theoretical available power (P) is given by (Mathew, 2006):

$$\boldsymbol{P = \frac{1}{2}\rho AV^3} \quad \textbf{(2)}$$

ISSN: 2408-7920

African Journal of Applied Research
Vol. 12, No. 3 (2026), pp. 315-340
http://www.ajaronline.com
https://doi.org/10.26437/ajar.v12
Received May 3, 2025
Peer reviewed: December 12, 2025
Revised: February 19, 2026
Published: April 2026

No turbine can generate all this power from wind. Thus, wind energy transfer efficiency affects turbine rotor power production (El-Askary et al., 2018). The power coefficient (CP) is the efficiency:

$$C_p = \frac{2P_T}{\rho_a A_T V^3} \quad (3)$$

The rotor blade profile, configuration, and setting affect the turbine's power coefficient. The designer must optimise these parameters to maximise CP at a wide range of wind velocities. Rotors experience a propulsion force (F) as:

$$\mathbf{F} = \frac{1}{2}\rho_a A_T V^2 \quad (4)$$

While the rotor torque (T) can be expressed as:

$$T = \rho_a A_T V^2 R \quad (5)$$

In fact, the ratio of the actual torque produced by the rotor to the ideal torque is referred to as the torque coefficient (CT) (El-Askary et al., 2020). This is given by:

$$C_T = \frac{2T_T}{\rho_a A_T V^2 R} \quad (6)$$

where T_T is the actual torque produced by the rotor. The major non-dimensional parameter is called Tip Speed Ratio (TSR) or (λ), which is used to explain the variables impacting Savinous rotor performance. It is defined as a ratio of the rotor's tip speed to the wind velocity (V) (Jiang et al., 2020):

$$\mathbf{TSR} = \frac{\mathbf{R\omega}}{\mathbf{V}} = \frac{\mathbf{2\pi NR}}{\mathbf{V}} \quad (7)$$

Rotor power and torque vary with tip speed ratio. Optimal energy transfer (λ) provides the highest power coefficient (C_P max) for a given rotor. Use the following equation to find the power coefficient-tip speed ratio relationship:

$$C_P = \frac{2P_T}{\rho_a A_T V^3} = \frac{2T_T \omega}{\rho_a A_T V^3} \quad (8)$$

Thus, the tip speed ratio can be given by (Saad et al., 2021):

$$\frac{CP}{CT} = \frac{R\omega}{V} = TSR \quad (9)$$

Experimental Calculation

The mechanical power extracted by the turbine (turbine shaft power) is:

$$P_{\mathbf{turbine}} = T \cdot \omega \quad (10)$$

ISSN: 2408-7920

African Journal of Applied Research
Vol. 12, No. 3 (2026), pp. 315-340
http://www.ajaronline.com
https://doi.org/10.26437/ajar.v12
Received May 3, 2025
Peer reviewed: December 12, 2025
Revised: February 19, 2026
Published: April 2026

Were,

$$\boldsymbol{\omega = \frac{2\Pi N}{60}} \quad \textbf{(11)}$$

$$\boldsymbol{T = F.r} \quad \textbf{(12)}$$

And r is the radius at the bottom of spindle (r=11.5 mm). To evaluate the tip speed ratio, from (9) which ($\frac{R\omega}{V}$). Furthermore, the available wind power is

$$\boldsymbol{P_{wind} = \frac{1}{2}\rho_a A V^3} \quad \textbf{(13)}$$

Where ρ_a =1.225 kg/m^3 and A= 0.24 m^2. Finally, the power coefficient (efficiency) (Zemamou et al., 2017) is:

$$\boldsymbol{CP = \frac{P_{turbine}}{P_{wind}}} \quad \textbf{(14)}$$

And the power losses (unextracted wind power) can be expressed as:

$$\mathbf{P_{Losses} = P_{wind} - P_{turbine}} \quad \textbf{(15)}$$

Numerical Methodology

A numerical model was validated to simulate the aerodynamic performance of a two-bladed, vertical-axis Savonius wind turbine. In the scientific literature, Nasef et al. (2025); Kadhim et al. (2024); Shouman & Helal (2023) have published similar validation methods for Savonius turbines. Validation is essential to ensure that the numerical methodology, governing equations, boundary conditions, and algorithms accurately predict turbine behaviour (Alaidany, 2024). Compare current numerical results to experimental and numerical data in scientific literature to validate.

Computational Domain

A two-dimensional computational domain is employed, consisting of a rotating circular sub-domain enclosing the rotor and a stationary outer domain representing the ambient flow field. To minimise blockage effects, the inlet boundary is positioned 5D upstream of the rotor, while the outlet boundary is located 10D downstream. The top and bottom boundaries are treated as symmetry boundaries. The dimensions as shown in Figure and 5, the setup mesh in the fluid domain and the rotating domain.

ISSN: 2408-7920

African Journal of Applied Research
Vol. 12, No. 3 (2026), pp. 315-340
http://www.ajaronline.com
https://doi.org/10.26437/ajar.v12
Received May 3, 2025
Peer reviewed: December 12, 2025
Revised: February 19, 2026
Published: April 2026

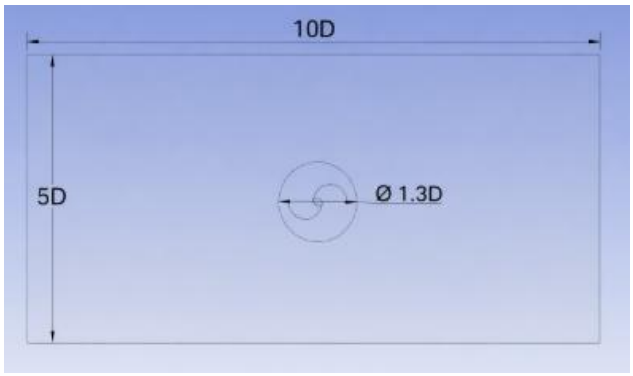

Figure 4: Computational domain and boundary conditions used in the validation study for (8, 6, and 4) inch.

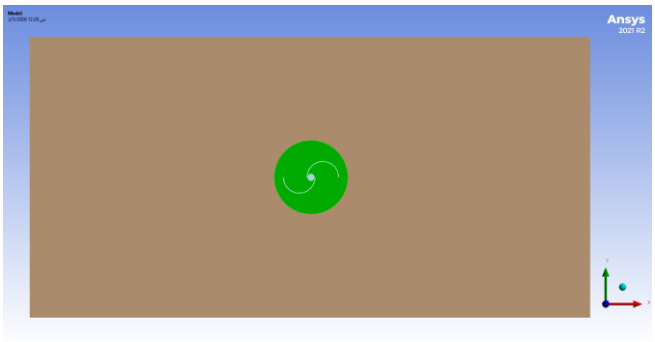

Figure 5: 2D computational domain 2-blade Savonius VAWT showing rotating and stationary regions.

Boundary Condition and Governing Equation

Inlets are velocity inlets with uniform wind speeds U, and outlets are pressure outlets with zero-gauge pressure. The dynamic mesh model controls blade surfaces as no-slip walls. Symmetry boundary conditions at the top and bottom represent an unbounded flow field. Savonius rotor simulations use numerical methods to solve the continuity equation and the unsteady, incompressible Reynolds-Averaged Navier–Stokes (RANS) equations (Tian et al., 2022). The SST k–ω turbulence model accurately models flow separation and unsteady wake structures in drag-based turbines.

$$\frac{\partial \rho}{\partial t} + \frac{\partial (\rho\, v^i)}{\partial x_i} = 0 \qquad (16)$$

$$\frac{\partial (\rho v'^i)}{\partial t} + \frac{\partial (\rho v'^i v'^j)}{\partial x_i} = -\frac{\partial p}{\partial x_i} + \frac{\partial}{\partial x_i}\mu\left[\frac{\partial v'^i}{\partial x_j} + \frac{\partial v'^j}{\partial x_i} - \left(\frac{2}{3}\right)\delta_{ij}\frac{\partial v'^l}{\partial x_l}\right] + \frac{\partial}{\partial x_i}(\rho\, v'iv'j) + F_i \qquad (17)$$

In these equations, ρ represents the fluid density, vi corresponds to the velocity components, p signifies the total pressure, Fi denotes the external body force components, and μ is the dynamic viscosity. The velocity vi can be expressed as the sum of the time-averaged value υ′ and the

ISSN: 2408-7920

African Journal of Applied Research
Vol. 12, No. 3 (2026), pp. 315-340
http://www.ajaronline.com
https://doi.org/10.26437/ajar.v12
Received May 3, 2025
Peer reviewed: December 12, 2025
Revised: February 19, 2026
Published: April 2026

fluctuating component vi'. The Shear Stress Transport (SST) k-ω turbulence model is chosen to model the turbulence terms of the RANS equations (Shkhair et al., 2022). The turbulent kinetic energy (k) and specific dissipation rate (ω) are computed using the following equations:

$$\frac{\partial}{\partial t}(\rho k) + \frac{\partial}{\partial x_i}(\rho k\, u_i) = \frac{\partial}{\partial x_j}\left[\left(\Gamma_k \frac{\partial \omega}{\partial x_j}\right) + G_k - Y_k + S_k\right] \quad (18)$$

$$\frac{\partial}{\partial t}(\rho \omega) + \frac{\partial}{\partial x_i}(\rho \omega\, u_i) = \frac{\partial}{\partial x_j}\left[\left(\Gamma_\omega \frac{\partial \omega}{\partial x_j}\right) + G_\omega - Y_\omega + D_\omega + S_\omega\right] \quad (19)$$

In these equations, Gk and Gω represent the generation of k and ω due to turbulent mean-velocity gradients, respectively; Γk and Γω denote the effective diffusivity; Yk and Yω indicate the dissipation of k and ω due to turbulence; Dω refers to the cross-diffusion term; and Sk and Sω are user-defined source terms.

Computational Mesh Generation and Dynamic Rotor Modelling

The dynamic mesh technique mathematically resolves the rotor motion to accurately simulate the highly unsteady, periodic, and massively separated flow fields of Savonius turbines. The dynamic sliding mesh updates the computational grid at each time step to represent rotor displacement, unlike steady state-based approximations like the Multiple Reference Frame (MRF) model, which often fail to represent transient aerodynamic phenomena in drag-based vertical axis turbines (Rizk & Nasr, 2023). The rotating inner subdomain has a rigid body angular velocity (weak rotation, no deformation) that matches the targeted tip speed ratio (l). Smoothing using diffusion and local remesh algorithms, following the relevant ANSYS Fluent numerical frameworks for rotating machinery, maintains grid quality and avoids negative cell volume in continuous rotation (Islam et al., 2013).

The stationary and rotating domains use a high-density unstructured triangular mesh for spatial discretisation. We use a detailed mesh and structured layers adjacent to all blade surfaces to capture the effects of the viscous sublayer, aerodynamic drag, and boundary-layer separation. Figure 6 depicts the fluid and rotating domain topology.

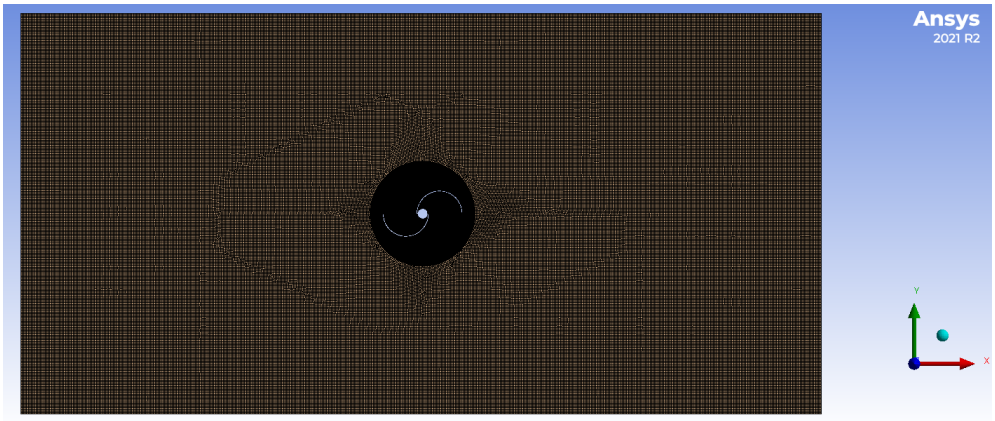

Figure 6: Detailed view of the computational grid, illustrating the unstructured mesh distribution within the stationary fluid domain and the refined rotating sub-domain.

ISSN: 2408-7920

African Journal of Applied Research
Vol. 12, No. 3 (2026), pp. 315-340
http://www.ajaronline.com
https://doi.org/10.26437/ajar.v12
Received May 3, 2025
Peer reviewed: December 12, 2025
Revised: February 19, 2026
Published: April 2026

Furthermore, to ensure the numerical predictions are free from the spatial discretisation errors, a strict grid independence study was performed for the varied rotor scales. The optimised configurations (mesh-independent) resulted in element counts of 332,034, 174,606 and 128,416 elements for the 8-inch, 6-inch and 4-inch rotor models, respectively. The unique meshing profiles for these three geometrical scales are shown in Figure .

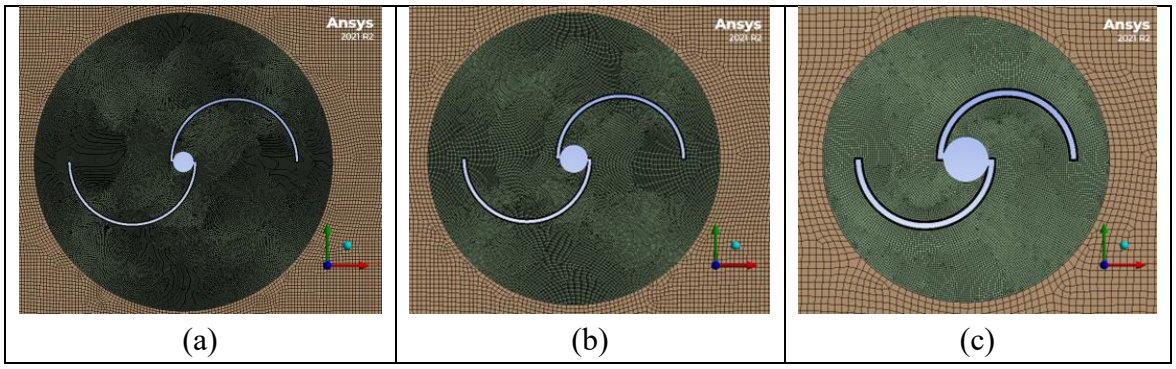

Figure 7: Cross-sectional mesh topologies for the evaluated Savonius rotor scales: (a) 8-inch, (b) 6-inch, and (c) 4-inch models, highlighting the near-wall inflation layers and element densities.

RESULTS AND DISCUSSION

This section includes a detailed review of the Savonius vertical-axis wind turbine, designed to generate wind energy from cars. To guarantee a comprehensive and well-structured analysis, the discussion is clearly divided into three main parts, which are: (1) Numerical Simulation and Flow Visualization, providing an explanation of the basic aerodynamic behaviors and wake patterns; (2) Experimental Parametric Analysis, providing a measurement of the actual power and torque coefficients for different shapes; and (3) Experimental-Numerical Validation, providing a confirmation of the real-world results with high support of the high aerodynamic efficiency achieved with the low-friction spindle mechanism.

Simulation Results, Visualisation and Analysis of Flow Patterns

Before examining the actual power outputs, we performed preliminary 2D numerical simulations with ANSYS Fluent 2021-R1 to visually and mathematically decompose the complex fluid dynamics that affect the Savonius rotor. Using the SST k-ω turbulence model and dynamic mesh algorithms, these simulations approximate the chaotic, time-varying flow conditions in urban traffic wakes (4 to 8 m/s). The visual manifestation of the pressure and speed patterns is the key to understanding the essential aerodynamic processes - such as where the flow separates, regions of still air and the formation of vortices behind the rotor. By indicating changes in flow speed and pressure differences around the spinning blades, the CFD model shows where drag aids motion and where it slows it down. This supports the finding of Kothe et al. (2020).

ISSN: 2408-7920

African Journal of Applied Research
Vol. 12, No. 3 (2026), pp. 315-340
http://www.ajaronline.com
https://doi.org/10.26437/ajar.v12
Received May 3, 2025
Peer reviewed: December 12, 2025
Revised: February 19, 2026
Published: April 2026

To systematically analyse the scaling effects on the aerodynamic flow field, the visualisation analysis is divided into three different cases according to rotor blade diameters (8, 6, and 4) inch three wind speed (4, 6, and 8) m/s as follows:

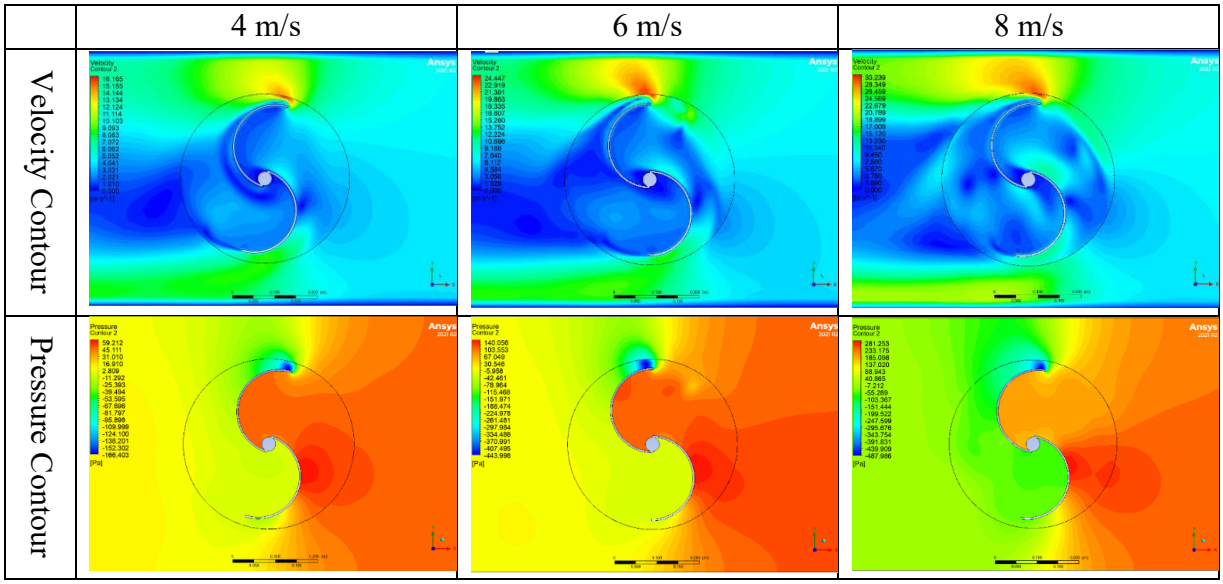

Figure 8: The Simulation Results of the Velocity and Pressure for 2 blades and 8-inch Diameter Blade.

In Case 1, with a blade diameter of 8 inches, Figure illustrated that CFD simulations reveal complex aerodynamic interactions of an 8-inch-diameter rotor. At low speeds, 4 m/s, an accelerated current and areas of high pressure arise on the convex blades, with a separation of the flux at the tips. Increasing the speed to 6 m/s increases the impact duration and generates an opposing torque from the pulling of the returning blades. At 8 m/s, the flow separation dominates and large vortices are formed, which expand the aerodynamic effect. Despite the increase in absolute torque due to dynamic compression, the losses increase significantly. This experimentally explains the low power factor (Cp) despite the high overall capacity, confirming the finding of Gao et al. (2025) that increasing the diameter enhances wind interception but reduces efficiency due to excess drag and energy loss in the impact.

ISSN: 2408-7920

African Journal of Applied Research
Vol. 12, No. 3 (2026), pp. 315-340
http://www.ajaronline.com
https://doi.org/10.26437/ajar.v12
Received May 3, 2025
Peer reviewed: December 12, 2025
Revised: February 19, 2026
Published: April 2026

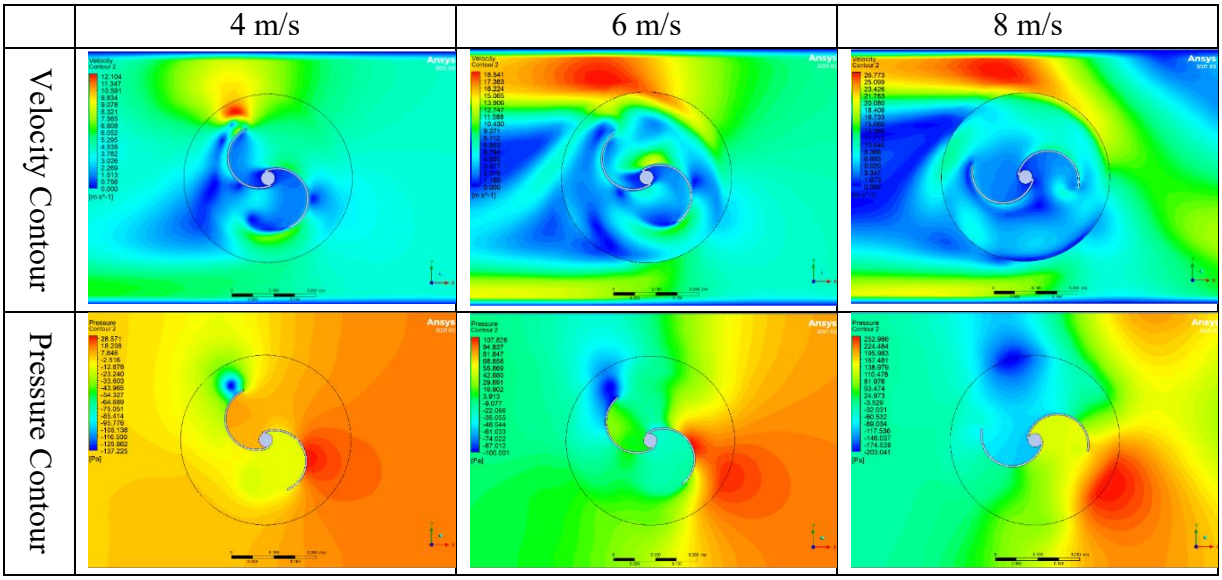

Figure 9: The Simulation Results of the Velocity and Pressure for 2 blades and 6-inch Diameter Blade.

In Case 2, the blade diameter 6-inch, Figure illustrated and analysis of a rotor with a diameter of 6 inches reveals a more balanced pneumatic performance compared to larger ones. At 4 m/s, the flow appears smooth with uniform acceleration and moderate trace formation. With an increase in speed to 6 m/s, the flow separation remains limited, and the vortices become weaker, improving torque stability. At 8 m/s, the impact remains confined with better re-adhesion of the runoff. This explains the experimentally improved Cp in some 6-inch diameter Blade configurations, achieving an optimal balance between wind energy interception and drag coefficient, reducing impact expansion and improving energy extraction efficiency.

ISSN: 2408-7920

African Journal of Applied Research
Vol. 12, No. 3 (2026), pp. 315-340
http://www.ajaronline.com
https://doi.org/10.26437/ajar.v12
Received May 3, 2025
Peer reviewed: December 12, 2025
Revised: February 19, 2026
Published: April 2026

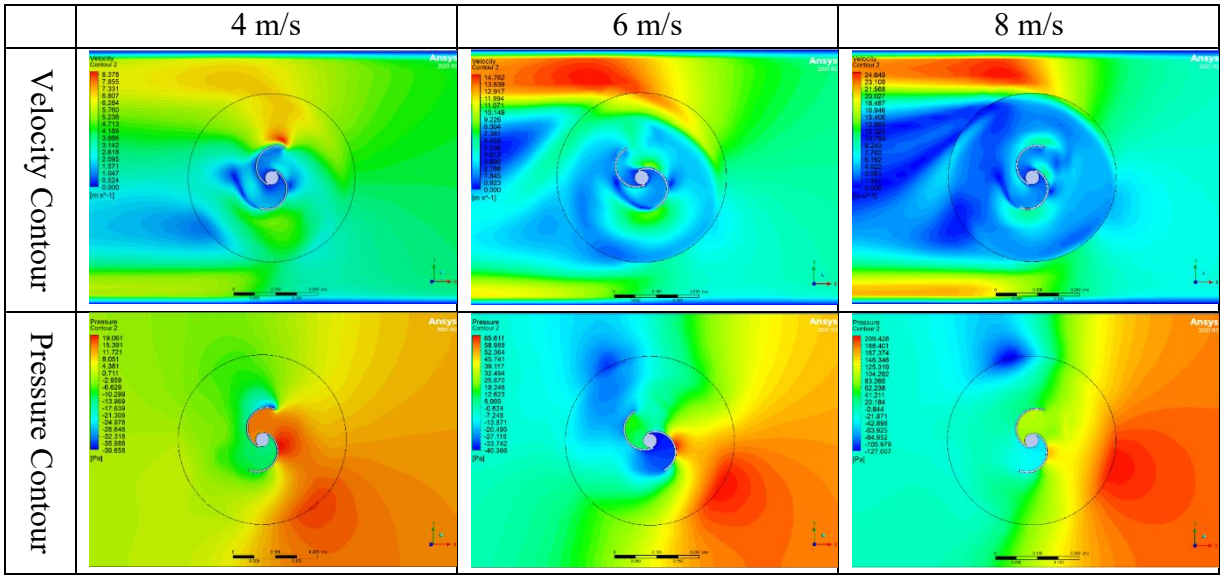

Figure 10: The Simulation Results of the Velocity and Pressure for 2 blades and 4-inch Diameter Blade.

In Case 3 the blade diameter 4-inch, Figure illustrates and analyses that the 4-inch-diameter rotor has the best flowability among the three cases. At 4 m/s, a limited separation of the flux and a small trace area appear. By increasing the speed, the trace remains compressed and symmetrical with weaker vortices. The pressure distribution produces an effective pressure difference with less counter torque thanks to the reduced area. Despite the increased separation at 8 m/s, vortices remain limited, which improves efficiency Cp and reduces drag. This enhances its superior aerodynamic efficiency and reduces impact losses, but its small area limits the total power generated compared to larger diameters.

Comparative Flow Behaviour Analysis

A comparative synthesis of the transient flow fields on the three scales of the rotor reveals a non-linear parabola between the geometric sizing of the rotor and its aerodynamic efficiency. The 8-inch rotor, although giving maximum swept area for absolute power generation, is severely penalised by massive flow separation, aggressive vortex shedding and extreme drag losses in its expanded wake region. On the other hand, the 4-inch rotor has the smallest wake and the lowest parasitic drag, but the critical low Reynolds number at which it operates affects the formation of a strong driving pressure differential, which affects energy extraction and peak efficiency.

ISSN: 2408-7920

African Journal of Applied Research
Vol. 12, No. 3 (2026), pp. 315-340
http://www.ajaronline.com
https://doi.org/10.26437/ajar.v12
Received May 3, 2025
Peer reviewed: December 12, 2025
Revised: February 19, 2026
Published: April 2026

The 6-inch rotor stands out as the absolute best aerodynamic compromise. It is able to achieve the right combination of adequate kinetic energy interception, well-controlled boundary layer separation, and stable torque generation. These flow visualisations rigorously support the empirical performance trends to be described in the following section, in that the maximum aerodynamic efficiency peak cap C sub p is reached at the intermediate 6-inch scale, proving that the aerodynamic efficiency doesn't scale linearly with the rotor diameter but rather reaches a peak efficiency at a critical fluid structure interaction threshold.

Experimental Results

This part presents a systematic quantification of the empirical performance of the Savonius rotor under the conditions of vehicle-induced winds. The analysis focuses on the performance of the Savonius rotor in terms of the power coefficient (Cp), saturation effect, mechanical power output (P_T) and internal power losses (P_L) as a function of the wind speed (V). The above parameters, taken together, determine the site-specific optimal configurations for urban energy harvesting applications.

Power Coefficient (Cp) versus Tip Speed Ratio (TSR)

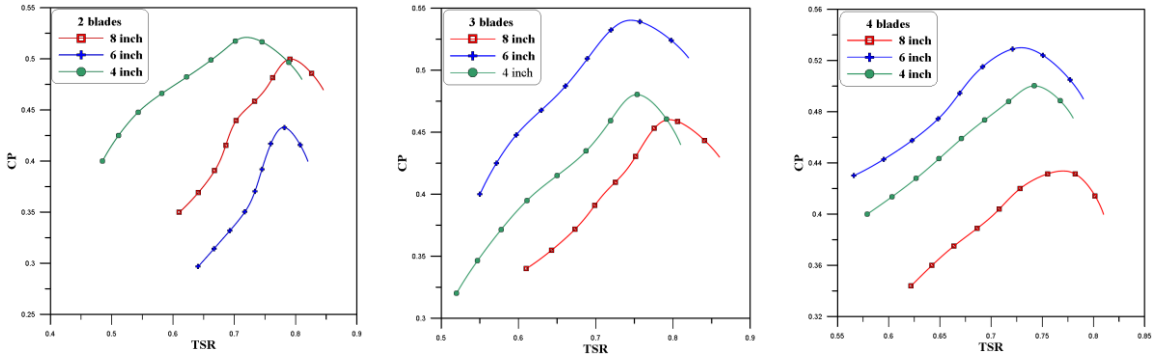

(a) (b) (c)

Figure 11: Power coefficient versus tip speed ratio for all VAWT cases (4, 6, and 8-inch) with 2, 3, and 4 blades, respectively.

The empirical variation of Cp versus l for the 2-, 3-, and 4-blade configurations is defined by Figure 11 (a-c). There is a clear parabolic trend in all shapes reaching a high point at the best TSR, followed by a decreasing trend due to aerodynamic stall and an increase in drag from the returning blade. The 2-blade, 4-inch rotor maximises high-speed efficiency by minimising drag resistance to a minimum. However, 3-blades, 6 inches, the best achievable performance (Cp = 0.545), which is well balanced between steady torque and on the other hand, 4-blades, 6, rotor, it is better in starting power at low speeds, although suffer more blockage problems, note the significant importance of this in the.

Saturation Phenomenon

The empirical performance curves invariably show a very different, non-linear, saturation curve, in which the power coefficient (Cp) rapidly declines as the TSR opt is exceeded. This critical

ISSN: 2408-7920

African Journal of Applied Research
Vol. 12, No. 3 (2026), pp. 315-340
http://www.ajaronline.com
https://doi.org/10.26437/ajar.v12
Received May 3, 2025
Peer reviewed: December 12, 2025
Revised: February 19, 2026
Published: April 2026

inflexion point represents the onset of "aerodynamic stall", which is the absolute physical limit of the rotor to convert the freestream kinetic energy to useful mechanical torque.

Two fluid-dynamic mechanisms are linked together that control this functional degradation. First of all, as the freestream velocity (V) increases, the parasitic pressure drag on the convex surface of the returning blade increases quadratically. This produces a great counter-torque, which tends to negate the positive driving momentum very quickly. Second, at elevated relative velocities, massive boundary layer separation occurs in the flow, leading to intense vortex shedding. This separated wake greatly reduces the incoming kinetic energy, which is wasted in turbulence and vibrations, rather than being converted into rotational speed. As a result, the rotor ends up in a balance state in which its weight and the strong drag forces prevent it from spinning faster along with the wind to keep its energy capture much lower than the maximum possible limit defined by the Betz limit.

Influence of Wind Velocity on Mechanical Power Generation (Pt)

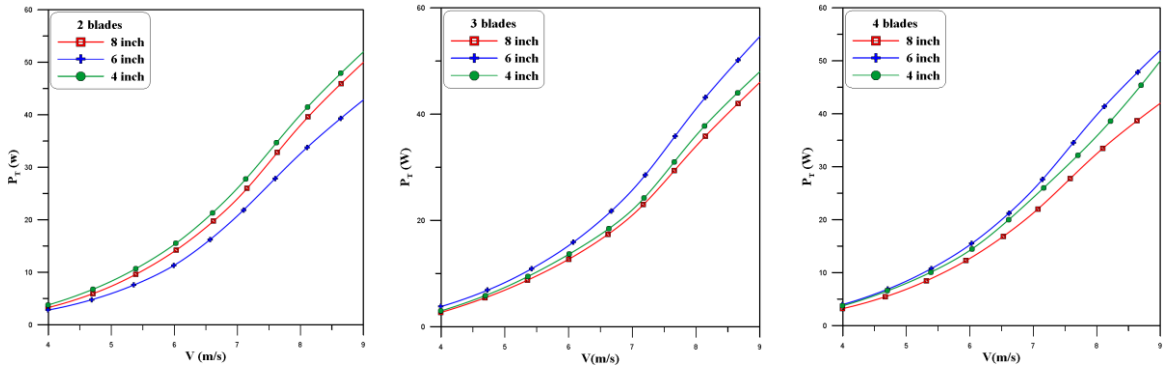

(a) (b) (c)

Figure 12: Variation of absolute mechanical power (Pt) as a function of freestream wind velocity (V) for the 2, 3, and 4-blade Savonius rotors.

All rotor designs are shown in Figure 12, which shows the relationship between the mechanical power produced (PT) and the wind speed (V). By fundamental aerodynamic theory, the extracted mechanical power is strictly cubically proportional to the wind speed, ($P_T \propto V^3$). In all the considered solidities (2, 3, and 4 blades), the 8-inch diameter rotor always generates the maximum mechanical power. This physical consequence is solely determined by the maximum cross-sectional area of the swept area, ultimately intersecting a much larger volumetric airflow, thus dominating its naturally reduced aerodynamic efficiency (Cp). Moreover, more blades (3 and 4 blades) have a significant effect on the low-velocity torque - enabling high self-starting rates - but they also come at a high price of parasitic drag in the higher velocities, which substantially rounds off the power growth curve. This is what defines a critical design trade-off: the 8-inch rotor is the one that optimises the raw energy capture, but the 6-inch rotor has the

ISSN: 2408-7920

African Journal of Applied Research
Vol. 12, No. 3 (2026), pp. 315-340
http://www.ajaronline.com
https://doi.org/10.26437/ajar.v12
Received May 3, 2025
Peer reviewed: December 12, 2025
Revised: February 19, 2026
Published: April 2026

merits of a critical strategic balance between large absolute power capture and maximum aerodynamic efficiency.

Velocity-Dependent Power Coefficient (C_p) Trends

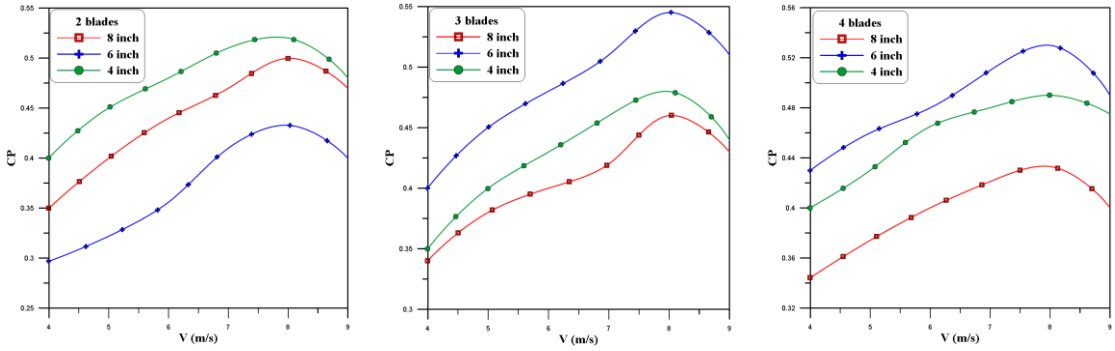

(a) (b) (c)

Figure 13: Power coefficient as a function of wind velocity for all VAWT cases (4, 6, and 8-inch) with 2, 3, and 4 blades, respectively.

The operational range of each rotor geometry is determined by the functional dependence of the aerodynamic efficiency of a rotor Cp on the freestream wind velocity (V) in Figure (a-c). In all configurations, Cp rises to a plateau with increasing wind speed, and thereafter attains an aerodynamic plateau due to the saturation mechanisms mentioned above. With the 2-blade rotors, the 4-inch diameter achieves optimum performance in its group by practically eliminating high-speed drag, whereas the 8-inch diameter is grossly ineffective due to increased profile losses across its larger overall surface area.

In the 3-blade subsystems, the 6-inch rotor will always achieve the highest Cp over the velocity envelope being tested. This particular geometry achieves the best aerodynamic compromise, effectively maximising the area swept and reducing the deep drag penalties that bring the 8-inch model to its knees, as well as the lack of energy capture of the 4-inch model.

The 4-blade designs, on the other hand, have a systemic decrease in the total levels of Cp in comparison with the 2 and 3-blade designs. The additional blades increase drag and block airflow, reducing overall performance. However, the 6-inch diameter is the most efficient within the high-solidity subset. It is the best geometrical trade-off for individual low-velocity urban microclimatic conditions that absolutely insist on high starting torque, even though it gives up maximum efficiency.

ISSN: 2408-7920

African Journal of Applied Research
Vol. 12, No. 3 (2026), pp. 315-340
http://www.ajaronline.com
https://doi.org/10.26437/ajar.v12
Received May 3, 2025
Peer reviewed: December 12, 2025
Revised: February 19, 2026
Published: April 2026

Power Losses (P_L) Analysis

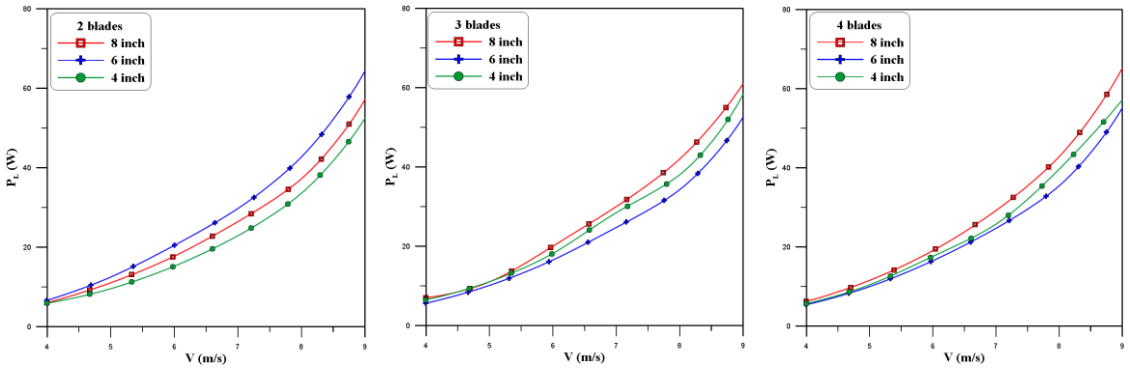

(a) (b) (c)

Figure 14: Variation of P_L as a function of V for the (a) 2-blade, (b) 3-blade, and (c) 4-blade Savonius rotors.

The work presents the variation of power losses (P_L) in the 2-, 3-, and 4-blade arrangements with wind speed (V) as in Figure (a-c). P_L is characterised by a gradual and increasing acceleration with increasing V across all solidities of the rotor. This physical action is essentially motivated by the quadratic growth of the parasitic force of drag on the returning blades and the kinetic energy, which is irretrievably lost in the turbulent wake.

The rotor of 8-inch size is geometrically the one that, in all the wind test regimes of the experiment, produces the greatest losses in power. This is a direct fluid-dynamic result of its expansive projected surface area, which greatly increases form drag and flow separation. Conversely, the rotor with the least aerodynamic losses is the 4-inch rotor since the profile of its front is minimal. Moreover, these losses are systematically multiplied by a shift of a 2-blade architecture to the 4-blade architecture because of the effect of increasing blockage and the increase counter-torque of the new returning blades. Finally, the 3-blade, 6-inch rotor turns out to be the final optimal aerodynamic tradeoff, carefully compromising on the high cost of excessive drag but at the same time maintaining the high-quality extraction of energy.

Efficiency Justification and Performance Benchmarking

To put it in mathematical perspective, the aerodynamic efficiency of the best setup (3-blade, 6-inch) must be compared with the current literature. The maximum power coefficient of Cp=0.545 was achieved, which was indeed excellent in the present study. Evidently, in stark contrast, recent strict parametric analyses of Savonius rotors describe much lower performance limits; an example of this is a peak Cp in (Francisco et al., 2025) of 0.242 and other highly optimised designs reached a plateau of 0.434 (Ogab et al., 2025).

This large difference is not occasioned by an experimental error, but by an underlying difference of methodology. Traditional experimental systems mechanically attach the test rotor to braking dynamometers of high-friction, massive. They therefore mistakenly incorporate large mechanical transmission losses as directly proportional to the reported aerodynamic Cp. The

African Journal of Applied Research
Vol. 12, No. 3 (2026), pp. 315-340
http://www.ajaronline.com
https://doi.org/10.26437/ajar.v12
Received May 3, 2025
Peer reviewed: December 12, 2025
Revised: February 19, 2026
Published: April 2026

rotor of this study was effectively decoupled from any intrinsic parasitic mechanical penalties by a purposeful design and execution of a custom near-zero-friction point-contact spindle. Consequently, the pure unattenuated aerodynamic coefficient of power is measured only by the isolated value 0.545. It alters the perception of the optimal output of the enhanced Savonius design operating in slow, turbulent airflows generated by vehicles, demonstrating that prior research by Dewan et al. (2021) has persistently underestimated the aerodynamic performance of drag-based rotors.

Experimental-Numerical Validation

The actual aerodynamic performance of this study is verified with the time-varying 2D computational fluid dynamics (CFD) analysis to guarantee the accuracy of this study. As indicated in Figure 20, there is a direct comparison of the experimental and numerical power coefficients (Cp) versus the TSR in the normal 2-blade design with rotor diameters of (8, 6, and 4) inches.

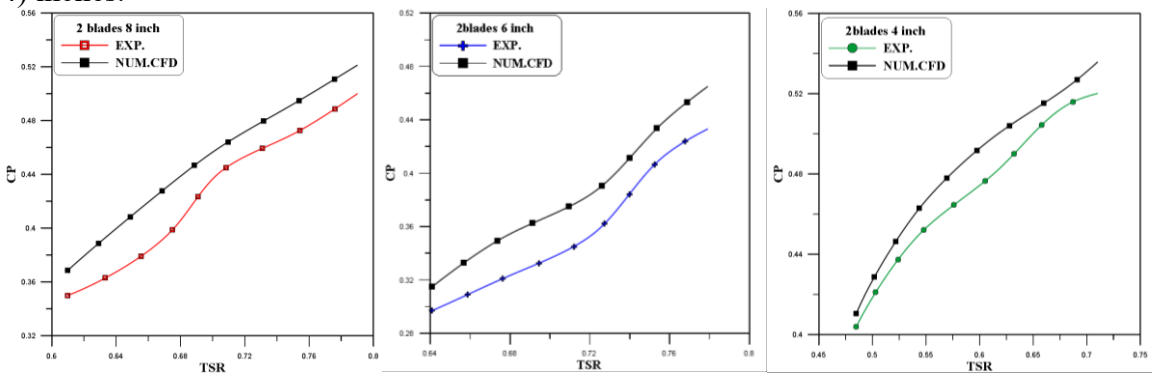

(a) (b) (c)

Figure 15: Comparison between EXP. and NUM. CFD for 2-blades and (8, 6, and 4) inch respectively.

Figure 15 shows an accurate comparison of the results of a practical (Experimental) and two-dimensional numerical simulation (CFD) of a two-feather Savonius fan with diameters of 4, 6, and 8 inches. The curves show excellent correspondence between the practical and numerical behaviours: as the TSR increases, Cp first increases to a maximum and then decreases, confirming the numerical model's accuracy in capturing dynamic saturation. It is noted that the numerical results follow the same general direction as the practical results, with an error margin of no more than 5-7%, indicating the efficiency of the SST-K-ω turbulence model used in the simulation. The 4-inch diameter shows the highest aerodynamic efficiency due to lower drag, while the 8-inch diameter shows the lowest power factor due to increased vortex formation and pressure loss behind the Blades. This close correspondence between the practical and numerical results validates the study's methodology and confirms the finding of Toudarbari et al. (2021) that the numerical model is reliable for the design and analysis of turbine performance in urban conditions, where wind speeds are influenced by vehicle traffic.

ISSN: 2408-7920

African Journal of Applied Research
Vol. 12, No. 3 (2026), pp. 315-340
http://www.ajaronline.com
https://doi.org/10.26437/ajar.v12
Received May 3, 2025
Peer reviewed: December 12, 2025
Revised: February 19, 2026
Published: April 2026

CONCLUSION

There is conclusive empirical evidence that the aerodynamic efficiency Cp) does not scale in a straight line with the diameter of the rotor or the velocity of the wind. Although the highest diameter (8-inch) has the highest absolute mechanical power ($P_T \propto V^3$), because of the area covered, it is aerodynamically crippled at high velocities. The transient CFD analysis reveals that such deterioration in performance is due to large separation of the boundary layer and more vortex shedding that consumes kinetic energy.

The 6-inch 3-blade rotor design was the ultimate aerodynamic tradeoff. It effectively overcomes the energy capture limitation of the 4-inch models, as well as countering the excessive parasitic drag of the 8-inch models. The design resulted in a record high power coefficient, Cp=0.545, making this theoretical high-power coefficient the new theoretical power ceiling of Savonius turbines in turbulent microclimates.

The study conclusively shows that a single so-called universal turbine design cannot work in urban energy collection. Optimising energy harvesting requires geometrical optimisation of the sites using localised wind profiles due to traffic. The best configurations are determined as follows for the three main arterial entrances of Hillah City;

- Entry 1: A 2-blade, 4-inch rotor is the best choice (Cp=0.48). It is not very solid, and thus, the drag of the returning blades caused by the high continuous traffic flows is minimised.
- Entry 2: The 3-blade, 6-inch rotor is best (Cp= 0.545). It offers the ultimate compromise between constant torque allocation and optimum aerodynamic efficiency.
- Entry 3: The 6-inch, 4-blade rotor is highly encouraged (Cp=0.528). With its reduced peak efficiency, it is very solid, giving it the necessary critical self-starting torque to get it started under intermittent, low-speed traffic conditions.

Ultimately, this study provides a valid and flexible blueprint of applying modified Savonius wind turbines to provide power to the local city systems, indicating that cautious design modifications are vital in achieving a successful wind energy harvesting, which is a product of human activities.

REFERENCES

Akhlaghi, M., & Ghafoorian, F. (2023). Investigation of Arc Angle Rotor Blade Variations Effect of Savonius Vertical Axis Wind Turbine on Power and Torque Coefficients Using a 3D Modeling. *Renewable Energy Research and Applications*, *4*(1), 13–19. https://doi.org/10.22044/rera.2022.11282.1084

Akwa, J. V., Vielmo, H. A., & Petry, A. P. (2012). A review on the performance of Savonius wind turbines. *Renewable and Sustainable Energy Reviews*, *16*(5), 3054–3064. https://doi.org/10.1016/j.rser.2012.02.056

Al-Gburi, K. A. H., Al-quraishi, B. A. J., Ismail Alnaimi, F. B., Tan, E. S., & Al-Safi, A. H. S. (2022). Experimental and Simulation Investigation of Performance of Scaled Model for a

African Journal of Applied Research
Vol. 12, No. 3 (2026), pp. 315-340
http://www.ajaronline.com
https://doi.org/10.26437/ajar.v12
Received May 3, 2025
Peer reviewed: December 12, 2025
Revised: February 19, 2026
Published: April 2026

Rotor of a Savonius Wind Turbine. *Energies*, *15*(23). https://doi.org/10.3390/en15238808

Al-Gburi, K. A. H., Alnaimi, F. B. I., Al-quraishi, B. A. J., Tan, E. S., & Kareem, A. K. (2023). Enhancing Savonius Vertical Axis Wind Turbine Performance: A Comprehensive Approach with Numerical Analysis and Experimental Investigations. *Energies*, *16*(10), 4204. https://doi.org/10.3390/en16104204

Alaidany, A. A. (2024). A Review of IoT-Based Wearable Sensor Systems for Healthcare Monitoring. *AMERICAN Journal of Engineering, Mechanics and Architecture*, *2*(5), 132–159. https://doi.org/10.13140/RG.2.2.18587.27684

Ali, M. H. (2013). Experimental comparison study for Savonius wind turbine of two & three blades at low wind speed. *International Journal of Modern Engineering Research (IJMER)*, *3*(5), 2978–2986.

Antar, E., & Elkhoury, M. (2019). Parametric sizing optimization process of a casing for a Savonius Vertical Axis Wind Turbine. *Renewable Energy*, *136*, 127–138. https://doi.org/10.1016/j.renene.2018.12.092

Blecich, P., Bonefačić, I., Senčić, T., & Wolf, I. (2025). Resilience Under Heatwaves: Croatia's Power System During the July 2024 Heatwave and the Role of Variable Renewable Energy by 2030. *Applied Sciences*, *15*(12), 6440. https://doi.org/10.3390/app15126440

Chen, L., Chen, J., & Zhang, Z. (2018). Review of the Savonius rotor's blade profile and its performance. *Journal of Renewable and Sustainable Energy*, *10*(1). https://doi.org/10.1063/1.5012024

Dewan, A., Gautam, A., & Goyal, R. (2021). Savonius wind turbines: A review of recent advances in design and performance enhancements. Materials Today: Proceedings, 47, 2976-2983.

Dhoble, L. N., & Mahalle, A. K. (2016). CFD analysis of Savonius vertical axis wind turbine: a review. International Research Journal of Engineering and Technology, 3(01), 958-962.

Ebrahimpour, M., Shafaghat, R., Alamian, R., & Safdari Shadloo, M. (2019). Numerical Investigation of the Savonius Vertical Axis Wind Turbine and Evaluation of the Effect of the Overlap Parameter in Both Horizontal and Vertical Directions on Its Performance. *Symmetry*, *11*(6), 821. https://doi.org/10.3390/sym11060821

El-Askary, W. A., Saad, A. S., AbdelSalam, A. M., & Sakr, I. M. (2018). Investigating the performance of a twisted modified Savonius rotor. *Journal of Wind Engineering and Industrial Aerodynamics*, *182*, 344–355. https://doi.org/10.1016/j.jweia.2018.10.009

El-Askary, W. A., Saad, A. S., AbdelSalam, A. M., & Sakr, I. M. (2020). Experimental and Theoretical Studies for Improving the Performance of a Modified Shape Savonius Wind Turbine. *Journal of Energy Resources Technology*, *142*(12), 121303. https://doi.org/10.1115/1.4047326

El-Ghazali, A. (2016). *The influence of turbine geometry on the performance of c-section vertical axis wind turbine*. Doctoral dissertation, Master's thesis, Near East University.

Faleh, M. A., Abdulsada, A. M., Alaidany, A. A., Al-shareeda, M. A., Amin, M., & Shehab, R. (2025). *SECRE-MEN : A Lightweight Quantum-Resilient Authentication Framework for IoT-Edge Networks*. *6*(4), 1681–1692. https://doi.org/10.18196/jrc.v6i4.26006

Fanel Dorel, S., Adrian Mihai, G., & Nicusor, D. (2021). Review of Specific Performance Parameters of Vertical Wind Turbine Rotors Based on the SAVONIUS Type. *Energies*,

African Journal of Applied Research
Vol. 12, No. 3 (2026), pp. 315-340
http://www.ajaronline.com
https://doi.org/10.26437/ajar.v12
Received May 3, 2025
Peer reviewed: December 12, 2025
Revised: February 19, 2026
Published: April 2026

14(7), 1962. https://doi.org/10.3390/en14071962

Farajyar, S., Ghafoorian, F., Mehrpooya, M., & Asadbeigi, M. (2023). CFD investigation and optimization on the aerodynamic performance of a Savonius vertical axis wind turbine and its installation in a hybrid power supply system: A case study in Iran. *Sustainability*, *15*(6), 5318.

Farozan, I., & Indartono, Y. S. (2024). An Experimental Study on the Performance of Check Valve-Aided Savonius Wind Rotors with Semi-Circular Blade. *International Journal of Technology*, *15*(6), 1923–1935. https://doi.org/10.14716/ijtech.v15i6.6110

Francisco, J., Rhakasywi, D., & Fahrudin, F. (2025). Experimental Analysis of the Performance of Savonius VAWT with Different Numbers of Blades on Roofs. *Indonesian Journal of Innovation Studies*, *26*(4), 1–7. https://doi.org/10.21070/ijins.v26i4.1675

Gao, X., Yang, Z., & James, S. (2025). Effects of wind barrier height and porosity on dust deposition and power generation efficiency of photovoltaic arrays. Solar Energy, 298, 113642.

Govind, B. (2017). Increasing the operational capability of a horizontal axis wind turbine by its integration with a vertical axis wind turbine. *Applied Energy*, *199*, 479–494. https://doi.org/10.1016/j.apenergy.2017.04.070

Gumilar, L., Kusumawardana, A., Habibi, M. A., Afandi, A. N., Prihanto, D., & Aji, A. F. (2019). Performance Analysis of Vertical Wind Turbine Type Savonius-L Based on Wind Speed, Rotation Speed, and Number of Blades. *2019 International Seminar on Application for Technology of Information and Communication (ISemantic)*, 383–388. https://doi.org/10.1109/ISEMANTIC.2019.8884302

Im, H., & Kim, B. (2022). Power Performance Analysis Based on Savonius Wind Turbine Blade Design and Layout Optimization through Rotor Wake Flow Analysis. *Energies*, *15*(24), 9500. https://doi.org/10.3390/en15249500

Islam, M. R., Mekhilef, S., & Saidur, R. (2013). Progress and recent trends of wind energy technology. *Renewable and Sustainable Energy Reviews*, *21*, 456–468. https://doi.org/10.1016/j.rser.2013.01.007

Ismail, K. A., Lino, F. A., Baracat, P. A., de Almeida, O., Teggar, M., & Laouer, A. (2025). Wind Turbines for Decarbonization and Energy Transition of Buildings and Urban Areas: A Review. Advances in Environmental and Engineering Research, 6(1), 1-59.

Jiang, Y., Zhao, P., Stoesser, T., Wang, K., & Zou, L. (2020). Experimental and numerical investigation of twin vertical axis wind turbines with a deflector. *Energy Conversion and Management*, *209*, 112588. https://doi.org/10.1016/j.enconman.2020.112588

Kadhim H. Suffer, & Yousif Abed Saleh Saleh. (2024). Numerical and Experimental Investigation of the Aerodynamic for the IceWind Blades VAWT. *International Journal of Scientific Research in Science, Engineering and Technology*, *11*(4), 139–146. https://doi.org/10.32628/ijsrset24114111

Karimi, O., Koopaee, M. K., reza Tavakolpour-Saleh, A., & Hosseini, S. E. (2023). *Investigating overlap ratio effect on performance of a modified Savonius wind turbine: An experimental study*.

Kothe, L. B., Möller, S. V., & Petry, A. P. (2020). Numerical and experimental study of a helical Savonius wind turbine and a comparison with a two-stage Savonius turbine. Renewable

African Journal of Applied Research
Vol. 12, No. 3 (2026), pp. 315-340
http://www.ajaronline.com
https://doi.org/10.26437/ajar.v12
Received May 3, 2025
Peer reviewed: December 12, 2025
Revised: February 19, 2026
Published: April 2026

Energy, 148, 627-638.

Kurniati, S., Syam, S., & Sanusi, A. (2023). Numerical investigation and improvement of the aerodynamic performance of a modified elliptical-bladed Savonius-style wind turbine. *AIMS Energy*, *11*(6), 1211–1230. https://doi.org/10.3934/energy.2023055

Mathew, S. (2006). *Wind energy: fundamentals, resource analysis and economics* (Vol. 1). Springer.

Meri Al Absi, S., Hasan Jabbar, A., Oudah Mezan, S., Ahmed Al-Rawi, B., & Thajeel Alattabi, S. (2021). An experimental test of the performance enhancement of a Savonius turbine by modifying the inner surface of a blade. *Materials Today: Proceedings*, *42*, 2233–2240. https://doi.org/10.1016/j.matpr.2020.12.309

Mohammadi, M., Lakestani, M., & Mohamed, M. H. (2018). Intelligent parameter optimization of Savonius rotor using Artificial Neural Network and Genetic Algorithm. *Energy*, *143*, 56–68. https://doi.org/10.1016/j.energy.2017.10.121

Montelpare, S., D'Alessandro, V., Zoppi, A., & Ricci, R. (2018). Experimental study on a modified Savonius wind rotor for street lighting systems. Analysis of external appendages and elements. *Energy*, *144*, 146–158. https://doi.org/10.1016/j.energy.2017.12.017

Naseem, A., Uddin, E., Ali, Z., Aslam, J., Shah, S. R., Sajid, M., Zaidi, A. A., Javed, A., & Younis, M. Y. (2020). Effect of vortices on power output of vertical axis wind turbine (VAWT). *Sustainable Energy Technologies and Assessments*, *37*, 100586. https://doi.org/10.1016/j.seta.2019.100586

Nasef, M. H., Asaad Awad, B. N., & EL-Askary, W. A. (2025). Installing new additional blades arrangement for improving Savonius rotor performance. In *Wind Engineering* (Vol. 49, Issue 2, pp. 536–556). https://doi.org/10.1177/0309524X241258478

Norouztabar, R., Mousavi Ajarostaghi, S. S., Mousavi, S. S., Nejat, P., Rahimian Koloor, S. S., & Eldessouki, M. (2022). On the Performance of a Modified Triple Stack Blade Savonius Wind Turbine as a Function of Geometrical Parameters. *Sustainability*, *14*(16), 9816. https://doi.org/10.3390/su14169816

Ogab, M., Norazmi, M. F., & Didane, D. H. (2025). Parametric Analysis of Blade Number Influence on the Aerodynamic Performance of a Savonius Rotor. *International Journal of Integrated Engineering*, *17*(4), 274–287. https://doi.org/doi.org/10.30880/ijie.2025.17.04.024

Prabowo, H., Wijayanto, D. S., Saputra, T. W., & Bakar, M. S. Bin. (2023). The Optimization of Savonius Helix Wind Turbine Cut-in Speed with the Variation of Blades-twist Rotor and Number of Blades. *JIPTEK*, *16*(2), 81. https://doi.org/10.20961/jiptek.v16i2.71389

Rahman, M. (2018). Numerical and experimental investigation of aerodynamic performance of vertical-axis wind turbine models with various blade designs. *Journal of Power and Energy Engineering*.

Rizaldi, T., & Brahmana, N. S. (2024). Performance Analysis of 2 U-Type Savonius Blades for Vertical Rotor Wind Turbine. *IOP Conference Series: Earth and Environmental Science*, *1302*(1), 012110. https://doi.org/10.1088/1755-1315/1302/1/012110

Rizk, M., & Nasr, K. (2023). Computational fluid dynamics investigations over conventional and modified Savonius wind turbines. *Heliyon*, *9*(6), e16876. https://doi.org/10.1016/j.heliyon.2023.e16876

ISSN: 2408-7920

African Journal of Applied Research
Vol. 12, No. 3 (2026), pp. 315-340
http://www.ajaronline.com
https://doi.org/10.26437/ajar.v12
Received May 3, 2025
Peer reviewed: December 12, 2025
Revised: February 19, 2026
Published: April 2026

Roy, S., & Saha, U. K. (2013). Investigations on the Effect of Aspect Ratio Into the Performance of Savonius Rotors. *ASME 2013 Gas Turbine India Conference*, *35161*, V001T07A002. https://doi.org/10.1115/GTINDIA2013-3729

Saad, A. S., Elwardany, A., El-Sharkawy, I. I., Ookawara, S., & Ahmed, M. (2021). Performance evaluation of a novel vertical axis wind turbine using twisted blades in multi-stage Savonius rotors. *Energy Conversion and Management*, *235*(November 2020), 114013. https://doi.org/10.1016/j.enconman.2021.114013

Shah, M. H., & Alsibiani, S. A. (2020). Design and construction of Savonius Rotor. *3c Tecnología: Glosas de Innovación Aplicadas a La Pyme*, *9*(1), 65–77. https://doi.org/id.org/0000-0003-2476-5887

Shkhair, M. M., Jaber, O. K., & Al Absi, S. M. (2022). Effect of rotor blades number and rotor position on the performance of a diffuser augmented wind turbine. *Int. J. Mech. Eng. Robot. Res*, *11*, 858–864.

Shouman, M. R., & Helal, M. M. (2023). Numerical investigation of improvement of counter rotating Savonius turbines performance with curtaining and fin addition on blade. *Alexandria Engineering Journal*, *75*, 233–242. https://doi.org/10.1016/j.aej.2023.05.002

Sumiati, R., Dinata, U. G. S., & Saputra, D. A. (2024). Enhancing Savonius Rotor Performance With Zigzag Surface Investigated at Drag Force, Pressure, and Flow Visualization Analysis. *TEM Journal*, *13*(2), 866–874. https://doi.org/10.18421/TEM132-03

Tian, W., Ni, X., Mao, Z., & Wang, Y.-F. (2022). Study on the performance of a new VAWT with overlapped side-by-side Savonius rotors. *Energy Conversion and Management*, *264*, 115746. https://doi.org/10.1016/j.enconman.2022.115746

Toudarbari, S., Maghrebi, M. J., & Hashemzadeh, A. (2021). Evaluation of Darrieus wind turbine for different highway settings using CFD simulation. Sustainable Energy Technologies and Assessments, 45, 101077.

Utomo, I. S., Tjahjana, D. D. D. P., & Hadi, S. (2018). Experimental studies of Savonius wind turbines with variations sizes and fin numbers towards performance. *AIP Conference Proceedings*, *1931*. https://doi.org/10.1063/1.5024100

Velásquez, L., Rengifo, J., Saldarriaga, A., Rubio-Clemente, A., & Chica, E. (2025). Geometric Optimization of Savonius Vertical-Axis Wind Turbines Using Full Factorial Design and Response Surface Methodology. *Sci*, *7*(4), 154. https://doi.org/10.3390/sci7040154

Zemamou, M., Aggour, M., & Toumi, A. (2017). Review of savonius wind turbine design and performance. *Energy Procedia*, *141*, 383–388. https://doi.org/10.1016/j.egypro.2017.11.047

Zemamou, M., Toumi, A., Mrigua, K., & Aggour, M. (2019). Modified Design of Savonius Wind Turbine Blade for Performance Improvement. *International Journal of Innovative Technology and Exploring Engineering*, *9*(1), 1432–1437. https://doi.org/10.35940/ijitee.A4202.119119

ISSN: 2408-7920